Rolling the Dice on the Delayed-Choice Quantum Eraser

Thomas V. Higgins

Abstract

This paper offers an alternative interpretation of the delayed-choice quantum eraser using the analogy of tossing two quantumly entangled dice. This interpretation duplicates the symmetric and antisymmetric data plots of the original paper by Kim et al. and provides a deeper insight into the statistical nature of the experiment. In particular, it proposes a stochastic explanation for why the original coincidence-detection plots do not go to zero where theory predicts they should be zero. In so doing, it also presents a simple metaphor of the experiment as a collection of random dice throws.

Published by tvhiggins.com December 29, 2025

Introduction

It was Albert Einstein himself who famously signaled his skepticism of quantum mechanics with the quote "God does not play dice with the world." With this one declaration he tossed aside the uncomfortable indeterminacy of the quantum world for the more familiar determinism of classical physics. Einstein never did make peace with quantum mechanics, and he repeated his dice metaphor throughout his life. But the quantum description of physical reality prevailed, and it now forms our most complete and accurate understanding of the universe.

To be clear, quantum mechanics is not for the faint-of-heart. It's a theory that flies in the face of our classical intuitions. But there are two experiments in particular that convincingly demonstrate two of the most bizarre yet fundamental effects of quantum behavior: superposition and entanglement. The two experiments are Young's renowned double-slit experiment (superposition) and the now famous delayed-choice quantum eraser (superposition and entanglement), which is a 21st-Century update of Young's experiment.

This paper examines the delayed-choice quantum eraser experiment of Kim et al. by equating it with the random throws of two dice. The metaphor not only seems to explain the data plots of the experiment, but this interpretation also offers a deeper understanding of its random, stochastic nature.

The experimental setup of Kim et al.

I already have given a fuller description of the physics behind the delayed-choice quantum eraser, which I published in March 2025 on my website. [1] Figure 1 of that paper (and this one) shows the basic experimental setup (see Figure 1).

At the bottom of Figure 1, UV light (351.1-nm) from an argon-ion laser (blue arrows) irradiates a double-slit, just like in Young's classic experiment. However, the similarity to Young's experiment quickly disappears next, because the wavefunction of each coherent UV photon that passes through the two slits is promptly used to pump two regions of a β-Barium Borate (BBO) crystal (labeled 1 and 2 in the figure).

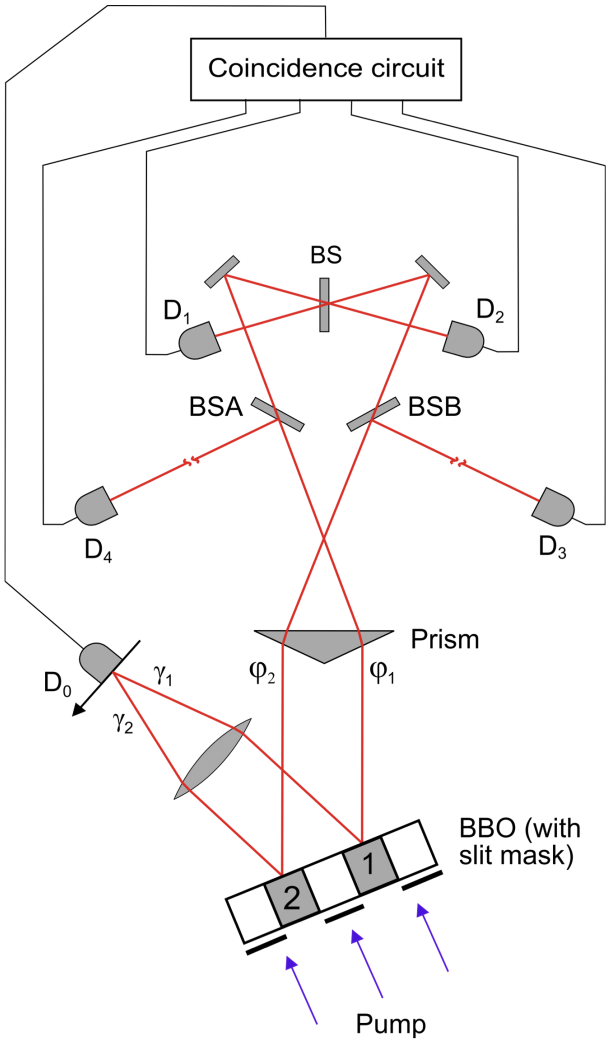

Figure 1

A tiny minority of pump photons (1 in 10^6) are transformed within the crystal into two entangled photons (signal γ and idler φ), each having twice the wavelength (702.2 nm) and therefore half the frequency or energy.

Signal photons (γ) emitted from the two BBO regions are directed off to the left in Figure 1 where they encounter a lens that focuses them onto the scanning detector D_0. This detector looks for any intensity variations that might appear along the focal plane where the two beams intersect.

Idler photons (φ) exit the BBO to a separate area of the setup in Figure 1, where they encounter a prism, three beamsplitters (BSA, BSB, BS), two mirrors, and four detectors (D_1, D_2, D_3, D_4). Optical path lengths from the BBO to these four detectors D_φ (φ=1-4) are all made equal, but they also are intentionally made longer than the optical path length from the BBO to D_0. This creates a time delay between the detections of each idler photon and its entangled signal-photon twin. In the original experiment, this delay amounts to "at least 8 ns."

Each of the D_φ detectors is also electronically linked with D_0 for coincidence detection (see Figure 1 again). Since each signal-idler pair is created simultaneously, coincidence detections will generate a ledger containing four subsets of synchronized event data. Each detection event at D_0 will therefore have a corresponding detection of its entangled twin 8 ns later at one of the four D_φ detectors.

The quantum-dice matrix

Here's how we might describe this experiment as the dice rolls of two four-sided dice: Each signal photon (γ) encountered by the scanning detector D_0 exists in a superposition of four quantum states (Ψ_1, Ψ_2, Ψ_3, and Ψ_4). These four wavefunctions represent: BBO regions 1 and 2 acting together symmetrically (Ψ_1); BBO regions 1 and 2 acting together antisymmetrically (Ψ_2); BBO region 2 acting alone (Ψ_3); and BBO region 1 acting alone (Ψ_4). Meanwhile, each signal-photon's entangled idler twin (φ) is randomly intercepted by either D_1, D_2, D_3, or D_4. (*There are important departures from this random detector distribution that will be introduced soon.*)

When D_0 detects a signal photon, the Copenhagen interpretation of quantum mechanics predicts a random wavefunction reduction from the four superposed states to a single state. The superposed wavefunction is said to "collapse" upon detection at D_0. This random wavefunction collapse at D_0 therefore might be modeled as the random outcome of a four-sided die. The random detections 8 ns later of each entangled idler twin at D_φ (where φ=1-4) could be thought of as the arbitrary outcomes of another four-sided die. Coincidence detections record the combinations of these correlated detections of the signal-idler pairs.

As such, the delayed-choice quantum eraser seems like a possible candidate for applying the statistical mathematics of tossing two four-sided dice. We start by building a matrix of all possible combinations of quantum detections, which would look like this:

$$\begin{pmatrix} \Psi_1 D_1 & \Psi_2 D_1 & \Psi_3 D_1 & \Psi_4 D_1 \\ \Psi_1 D_2 & \Psi_2 D_2 & \Psi_3 D_2 & \Psi_4 D_2 \\ \Psi_1 D_3 & \Psi_2 D_3 & \Psi_3 D_3 & \Psi_4 D_3 \\ \Psi_1 D_4 & \Psi_2 D_4 & \Psi_3 D_4 & \Psi_4 D_4 \end{pmatrix}$$

Matrix 1

In Matrix 1, Ψ_i (i = 1-4) symbolizes the four possible signal states detected first at D_0. The four idler detectors are denoted by rows D_j (j = 1-4). So there are 16 combinations (4 x 4) represented. Each row of combinations in the matrix represents all possible coincidence

detections involving a particular D_j idler detector, while each column lists the D_j distribution of coincidence detections that involve a specific signal wavefunction Ψ_i at D_0.

Applying the quantum-dice matrix to the experiment

In a fair toss of two four-sided dice, the 16 possible outcomes are entirely independent of each other. But in the delayed-choice quantum eraser, the distribution of coincidence detections is more complex. We must, therefore, modify our matrix to match the experimental conditions.

First, there are four impossible combinations in the experiment. Specifically, the coincidence detections $\Psi_1 D_2$ and $\Psi_2 D_1$ cannot occur because of the sorting property of the Mach-Zehnder quantum eraser, whereby D_1 cannot detect antisymmetric Ψ_2 photons, and D_2 cannot detect symmetric Ψ_1 photons. [1] $\Psi_3 D_4$ also is impossible because D_4 isn't even looking at the Ψ_3 wavefunctions coming exclusively from BBO region 2, so it can't detect them (refer to Figure 1). The same goes for $\Psi_4 D_3$, since D_3 isn't looking at BBO region 1, either. Therefore, these four coincidence detections must be set to zero in the matrix, like so:

$$\begin{pmatrix} \Psi_1 D_1 & 0 & \Psi_3 D_1 & \Psi_4 D_1 \\ 0 & \Psi_2 D_2 & \Psi_3 D_2 & \Psi_4 D_2 \\ \Psi_1 D_3 & \Psi_2 D_3 & \Psi_3 D_3 & 0 \\ \Psi_1 D_4 & \Psi_2 D_4 & 0 & \Psi_4 D_4 \end{pmatrix}$$

Matrix 2

The 12 remaining combinations in Matrix 2 represent the possible random coincidence detections in the experiment. *It is important to note here that while the idler detection probability at the available D_j detectors is still completely random (one-in-three odds, now), the detection probability of the entangled signal-photon twins at detector D_0 depends on the detector's position and the detected wavefunction Ψ_i, which alters the joint-detection rates of the signal-idler pairs accordingly. D_0 signal (Ψ_i) detections, which comprise half of the signal-idler joint detections, are evenly (randomly) distributed among the allowed D_j idler joint detections, and any detection without a corresponding signal or idler twin detection is ignored.*

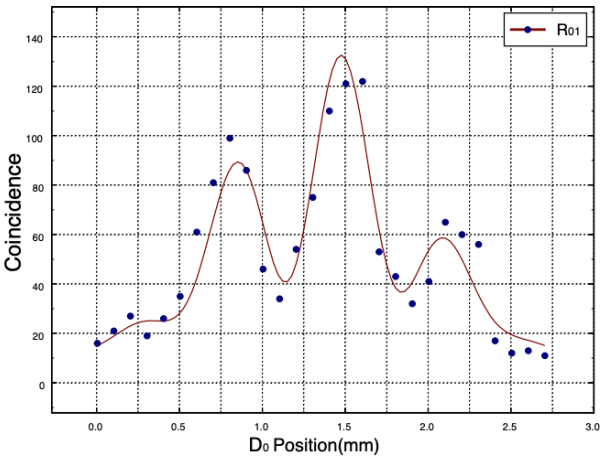

Figure 2 (from [2])

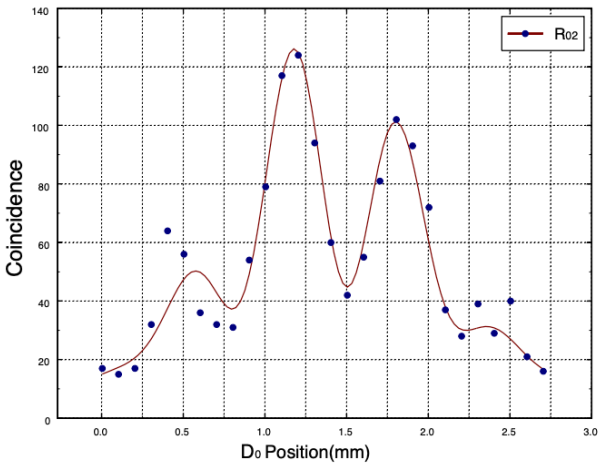

Figure 3 (from [2])

Notice, also, that coincidence detections involving D_1 (top matrix row) are not only paired with Ψ_1 signal-photon detections at D_0, but with the Ψ_3 and Ψ_4 photons as well. A similar effect can be seen in the other three rows of the matrix, too. Consequently, the data plots of coincidence detections should include all of these data. And, in fact, this is exactly what we see in the data plots presented in the original paper by Kim et al. (see Figures. 2 & 3). Their joint-detection curves ride above a conspicuous floor instead of going to zero where theory predicts. This key detail is neither explained nor acknowledged by the authors in the original paper. [2]

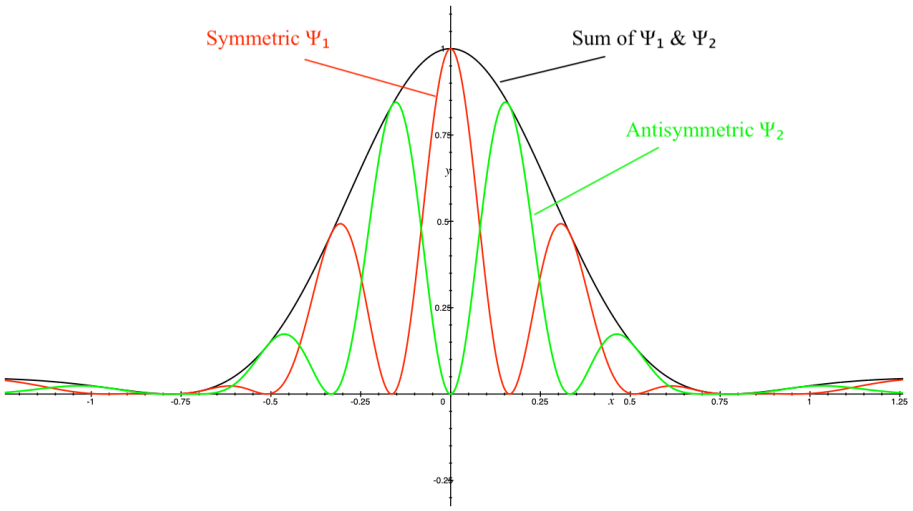

Figure 4

Standard theory predicts that the intensity (i.e. probability) plots of interfering symmetric and antisymmetric wavefunctions Ψ_1 and Ψ_2 (red and green plots in Figure 4 above) should periodically go to zero at specific locations in space. Clearly, this is not what we see in the symmetric and antisymmetric joint-detection plots of Figures 2 and 3. The disparity results from an accumulation of the other random joint detections shown in rows 1 and 2 of Matrix 2. These include $\Psi_3 D_1$, $\Psi_4 D_1$ in row 1 and $\Psi_3 D_2$, $\Psi_4 D_2$ in row 2; consequently, we should also include Ψ_3 and Ψ_4 probability waveforms to Figure 4, which I have done in Figure 5 (blue curves).

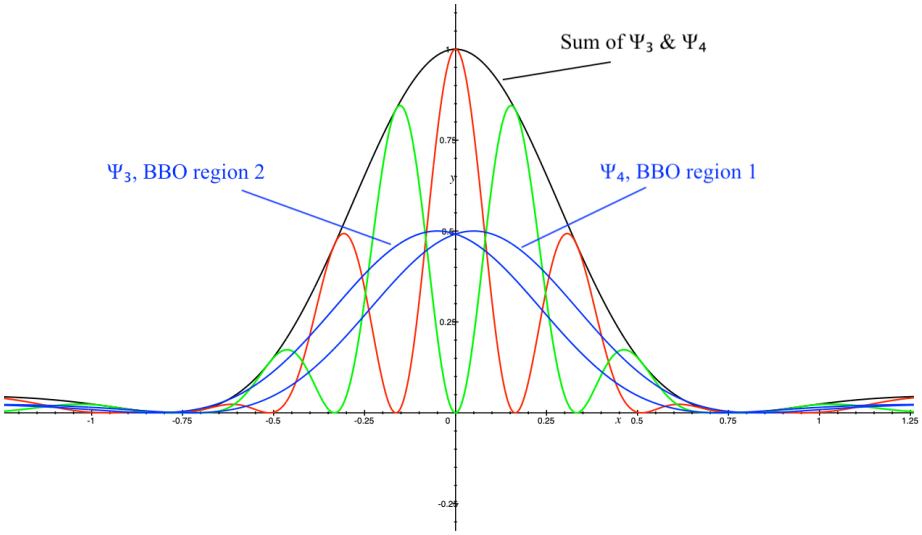

Figure 5

Now we can use the four theoretical intensities plotted in Figure 5 to estimate how much Ψ_3 and Ψ_4 contribute to the measured joint-detection rates plotted in Figures 2 and 3. (Even though the axes of Figure 5 don't match those of Figures 2 and 3, we can still use them. Just multiply the y-axis values of Figure 5 by 100.)

In the D_0 scanning plot of Figure 2, we see that its central maximum lies at the position of 1.5 mm, while the first minimum occurs at approximately 1.8 mm. We know from the corresponding red curve in Figure 5 that this minimum should be zero, but the lowest data point in Figure 2 shows a value of just over 30 at this minimum, so this must be the data floor level. The maximum, on the other hand, seems to be at about 125 or 130. Now, from the theoretical

plots of Ψ_3, and Ψ_4 in Figure 5 (blue curves), the joint detections at x = 0, which corresponds to the D_0 position of 1.5 mm in Figure 2, should each contribute a rate of about 50 (0.5 x 100).

For the D_0 antisymmetric plot of Figure 3, the minimum occurs at the same position (1.5 mm) as the symmetric maximum does in Figure 2, as expected. The antisymmetric maximum also looks to be about the same as the symmetric plot's maximum, 125 or 130, but at a position of 1.2 mm, instead. Let's see what we get when we use numbers based on the theoretical plots of Figure 5 for the entries of Matrix 2.

With an assumed joint-detection floor level of 30, the measured maximum rate of 130 for $\Psi_1 D_j$ and $\Psi_2 D_j$ in Figures 2 and 3 must actually be 100. We'll use this number for the theoretical maximum at the midpoint of 1.5 mm, which, again, corresponds to the y-axis (x = 0) in Figure 5. At this D_0 position, the Figure-5 rates for $\Psi_1 D_1$, $\Psi_2 D_1$, $\Psi_3 D_1$ and $\Psi_4 D_1$ in row 1 of Matrix 2 would be 100, 0, 50, 50. The second-row antisymmetric values of $\Psi_1 D_2$, $\Psi_2 D_2$, $\Psi_3 D_2$, and $\Psi_4 D_2$ would be 0, 0, 50, 50. Row 3 is 100, 0, 50, 0, and row 4 is 100, 0, 0, 50. (See Matrix 3.)

$$\begin{pmatrix} 100 & 0 & 50 & 50 \\ 0 & 0 & 50 & 50 \\ 100 & 0 & 50 & 0 \\ 100 & 0 & 0 & 50 \end{pmatrix}$$

Matrix 3

The diagonal of Matrix 3 (red boxes), where the column and row indexes are equal (i = j), represents the joint-detection rates of each signal wavefunction Ψ_i with its matching idler detection ($\Psi_1 D_1$, $\Psi_2 D_2$, $\Psi_3 D_3$, $\Psi_4 D_4$). The off-diagonal entries represent the contributions from all of the other possible joint detections. Each row denotes all of the joint-detection rates involving a single idler detector—for example D_1 in the first row. *To find the combined joint-detection rate of all four* Ψ_i *wavefunctions that involve a single idler detector, we add the average value of the off-diagonal elements in that matrix row to the diagonal element of that same row.* In this way we account for the random "background" joint detections at the idler detector of interest. Also, bear in mind that each new D_0 position generates a whole new matrix of joint-detection rates.

The joint-detection rate of the symmetric state in Figure 2 is represented by the D_1 row of Matrix 3 (row 1). This consists of $\Psi_1 D_1$ plus the average contributions from the three off-diagonal joint detections ($\Psi_2 D_1$, $\Psi_3 D_1$ and $\Psi_4 D_1$). Thus we have 100 + (0 +50 + 50)/3 = 133.33, which is pretty close to the measured coincidence rate of approximately 130 given in Figure 2 at a D_0 position of x = 1.5 mm. So the estimated data floor of 30 does seem to yield some agreement with experiment when calculating the theoretical values for Matrix 3 from Figure 5.

Row 2 of Matrix 3 gives us the antisymmetric D_2 coincidence data for D_0 at x = 1.5 mm. This is 0 + (0 + 50 + 50)/3 = 33.33, which is not too far off from the value of 40 given in Figure 3 at x = 1.5 mm. However, it is virtually equal to the other antisymmetric minimum plotted around x = 0.75 mm in Figure 3. Unlike the theoretical values of Figure 5, the actual experimental data plotted in Figures 2 and 3 are a little asymmetric and skewed.

The original paper includes a plot of D_0-D_3 joint-detections, too, but for some reason it does not yield as close a match with the detection rates predicted by Matrix 3. According to the matrix, joint-detection rates involving D_3 (or D_4) at a D_0 position of 1.5 mm should be 50 + (100 + 0 + 0)/3 = 83.33. But the original paper lists a joint-detection rate of about 118 for D_0-D_3 at this position. I cannot explain this discrepancy without knowing more about how this data was obtained and plotted, but the theoretical detection probability for Ψ_3 (and Ψ_4) at this midway position is half that of Ψ_1, for example. Therefore, the detection rate of Ψ_3 signal photons at D_0 also should be half for a detector of a given quantum efficiency. And this same rate difference must necessarily apply to the correlated idler twins arriving at D_j detectors 8 ns later. The D_0-D_3 coincidence plot in the original paper should therefore reflect this detection-rate difference.

I have applied the same quantum-dice matrix strategy to the data of Figures 2 and 3 at D_0 positions other than the midpoint of 1.5 mm, and the results all come close to the experimental values. They even duplicate the decreasing floor level as D_0 moves away from 1.5 mm, an effect that can readily be seen in the figures. The data floor is not flat. It bows upward in the middle.

Review and conclusions

This interpretation of the delayed-choice quantum eraser experiment began by applying the analogy of tossing two four-sided dice. But this simple metaphor of a game of chance had to

be altered to fit the quantum conditions of the experiment. In particular, the four-sided die representing the quantum probabilities at detector D_0 does not yield the uniform distributions that a fair four-sided die would. Instead, it's a dynamically "loaded" quantum die with probabilities that vary according to each of the four possible wavefunctions and the die's location in space. Rather than one number in four appearing after each toss, the number that appears depends on where the die is tossed and which of the four wavefunctions it lands on. It's as if the odds of a craps game played in Las Vegas were completely different from the same game played in Atlantic City.

In addition, the second four-sided idler die became a three-sided die. (Yes, these do exist.) Four of the 16 possible combinations of our four-sided dice metaphor had to be eliminated because of the physical constraints imposed on the idler side of the experiment—specifically because of the sorting done by the quantum eraser at D_1 and D_2, and because of the selective behavior of the D_3 and D_4 detectors. Moreover, the idler die D_j is entangled with the signal die of D_0, so the joint-detection rates are directly influenced by what happens first at D_0. Consequently, each Ψ_i detection rate at D_0 is reflected in the three allowed D_j idler detectors in each column of the quantum-dice matrix of joint detections.

The result is a very strange game of chance with two quantumly entangled dice, which is what makes this interpretation so interesting. For one, it puts to rest the counterintuitive "retrocausal" interpretations of this experiment once and for all. And for another, it implies that the experiment—and indeed the world—could very well be just another crapshoot. Sorry, Albert.